Lipid Bilayer Disruption Induced by Amphiphilic Janus Nanoparticles: The Non-Monotonic Effect of Charged Lipids

Journal:	*Soft Matter*
Manuscript ID	SM-ART-12-2018-002525.R1
Article Type:	Paper
Date Submitted by the Author:	30-Jan-2019
Complete List of Authors:	Lee, Kwahun; Indiana University, Chemistry Yu, Yan; Indiana University, Chemistry;

SCHOLARONE™
Manuscripts

Lipid Bilayer Disruption Induced by Amphiphilic Janus Nanoparticles: The Non-Monotonic Effect of Charged Lipids

Kwahun Lee and Yan Yu*

Department of Chemistry, Indiana University, Bloomington, IN 47405, USA

*Corresponding author: yy33@indiana.edu

ABSTRACT

In this study, we report the complex effects of charged lipids on the interaction between amphiphilic Janus nanoparticles and lipid bilayers. Janus nanoparticles are cationic on one hemisphere and hydrophobic on the other. We show that the nanoparticles, beyond threshold concentrations, induce holes in both cationic and anionic lipid bilayers mainly driven by hydrophobic interactions. However, the formation of these defects is non-monotonically dependent on ionic lipid composition. The electrostatic attraction between the particles and anionic lipid bilayers enhances particle adsorption and lowers the particle concentration threshold for defect initiation, but leads to more localized membrane disruption. Electrostatic repulsion leads to reduced particle adsorption on cationic bilayers and extensive defect formation that peaks at intermediate contents of cationic lipids. This study elucidates the significant roles lipid composition plays in influencing how amphiphilic Janus nanoparticles interact with and perturb lipid membranes.

Introduction

The structural integrity of cell membranes is vital for cell viability and functions. It has been shown that a wide range of synthetic materials can disrupt this integrity. Such findings have aroused great interest in assessing the possible adverse impact of engineered materials on biological systems,[1-6] as well as developing materials that disrupt cell membranes purposefully for biomedical applications, such as gene delivery.[3, 7-12] Much of this interest has focused specifically on nanoparticles,[13-20] polymers,[17, 21-26] and pore-forming peptides.[17, 27-32] Although these materials are very different from one another, their disruptive effects on biomembranes result from the same fundamental electrostatic and hydrophobic interactions. The competition and interplay of electrostatic and hydrophobic forces determines the nature of their influence on biomembrane integrity. For example, the mechanism by which pore-forming peptides disrupt membranes can be tuned by altering their sequences.[33] Adsorption of oxide nanoparticles on lipid bilayers was also shown to vary depending on the ionic lipid composition and pH of the suspension medium.[34] It is, therefore, important to understand the different roles played by each of the two forces in interactions between materials and membranes.

The interactions between particles and lipid membranes have already been the subject of intensive study. In elucidating the effect of electrostatic interactions, studies have shown drastically different effects of cationic versus anionic charges of nanoparticles on the integrity and structural rearrangement of lipid membranes.[35-39] In particular, cationic nanoparticles were found to be more disruptive to lipid membranes than anionic ones, even though the exact nature of the defects could vary depending on many factors such as surface charge density and particle size.[20, 40-46] Hydrophobic attraction between nanoparticles and lipid membranes has also been shown to drive the instability of lipid membranes in both experimental[13-16] and simulation studies.[47-54] So far, these studies have exclusively involved nanoparticles with chemically uniform surfaces. Recently, our group has explored chemically non-uniform nanoparticles, which present electrostatic and hydrophobic interactions that are spatially segregated on their surfaces.[9, 10] These amphiphilic nanoparticles have charges on one hemisphere and hydrophobic alkyl chains on the other. Because of the two-faced feature, they are called Janus particles. We found that they induce holes in zwitterionic lipid bilayers in the pM concentration range when their uniform counterparts exert negligible effect on the bilayers. Our research showed that hydrophobic interactions drive the formation of these holes through lipid extraction from the bilayers. Electrostatic interaction between particles and bilayers, we found, promotes the initial contact of the particles with the membrane. One important question that remains unclear is how the presence of charged lipids in the bilayer affects this disruption process. The addition of charges makes the lipid bilayers better mimics of real cell membranes, and we expect it to result in more complex particle-membrane interactions that need to be characterized.

In this study, our objective is to investigate the interactions between amphiphilic cationic /hydrophobic Janus nanoparticles (+/pho JPs) and cationic and anionic lipid bilayers at varied charge compositions. We focus on two kinds of lipids: anionic 1, 2-dioleoyl-sn-glycero-3-phosphate (DOPA) and cationic 1, 2-dioleoyl-3-trimethylammonium-propane (DOTAP). We show that the +/pho JPs induce defects in both cationic and anionic lipid bilayers, but that defect formation depends on the ionic lipid composition of the bilayer in a complex non-monotonic way. In particular, we find that electrostatic effects from the charged lipids, either anionic or cationic, affect particle adsorption on bilayers, particle concentration threshold for initiating defect formation, and the extent and process of defect formation. While defects are mostly driven by the hydrophobic attraction between the amphiphilic particles and lipid bilayers, of the consequence of such interactions is significantly modified by the electrostatic effects of charged lipids.

Results and discussions

The glass-supported lipid bilayers used in this study consisted primarily of zwitterionic 1,2-dioleoyl-sn-glycero-3-phosphocholine (DOPC) lipids. Varied fractions of either anionic DOPA or cationic DOTAP

lipids were added. The amphiphilic Janus nanoparticles used display amine groups at a density of ≈ 2 amine groups/nm^2 on their cationic hemisphere and octadecanethiol (ODT) on their hydrophobic gold-coated hemisphere (**Fig. 1a and b**). They were ≈ 100 nm in diameter, and fabricated in the same way described for our previous research.[55] For simplicity, they are referred to as "+/pho JPs".

1. The effects of anionic lipids on the interaction between +/pho JPs and lipid bilayers

We first investigated the effect of anionic lipids on the interaction between +/pho JPs and lipid bilayers. For this purpose, DOPC bilayers containing 0 mol% to 10 mol% of DOPA were prepared in a phosphate buffer solution (pH = 7). To avoid aggregation of the +/pho JPs, buffer solution above the bilayer was then exchanged for de-ionized water. We observed that the bilayer morphology remained planar up to a 1% content of DOPA, but that 5% and 10% DOPA bilayers exhibited many protruding, hemisphere-shaped "cap" structures. These appeared as micron-sized circles in fluorescence microscope images (**Fig. 1c**). These cap structures have been previously reported to be rich in DOPA and their formation is thought to be driven by asymmetric ionic strength on the opposite sides of the lipid bilayers.[56] The morphology of the bilayers was examined again 70 min after the addition of +/pho JPs. We found that +/pho JPs induced holes in all DOPA bilayers. Because their morphology can vary, we refer to the holes as defects in general. However, different particle concentration thresholds were required to induce these defects depending on different charge content in bilayers. A 20 pM concentration of particles was necessary to cause visible defects in pure DOPC and 0.2% DOPA bilayers, but 15 pM was sufficient at 1% and higher DOPA content. The morphology of the defects also varied depending on the DOPA fraction. The defects appeared rounded with smooth edges in 5% and 10% DOPA bilayers, in contrast to the more branched defects in bilayers containing 1% or less DOPA. By measuring the associate rate constant (k_a) of the particle adsorption on the bilayers, we confirmed that the anionic charges in DOPA bilayers enhanced the adsorption rate of +/pho JPs (**Fig. S1**). The stronger electrostatic attraction produced by a higher fraction of DOPA cap structures likely leads to the lower threshold particle concentration for membrane disruption.

We next quantified the effect of +/pho JPs on the integrity of DOPA bilayers. The surface coverage of defects was measured in fluorescence images to quantify the extent and localization of defect formation. We found that bilayers with a 0.2-5% DOPA content exhibited less surface coverage of defects than pure DOPC bilayers in the presence of 20 pM particles (**Fig. 2a**). This was surprising, because one would expect that stronger particle adsorption caused by the anionic lipid should produce more membrane defects. In fact, the surface coverage of defects only changed slightly from 0.2% to 5% content of DOPA, but increased significantly for 10% DOPA. The observation that the defect coverage depended non-monotonically on DOPA content is further demonstrated in a color-coded phase diagram (**Fig. 2b**). It is clear that the threshold particle concentration for inducing bilayer defects is lowered at higher DOPA content, but the defect area does not follow the same relationship. We also quantified the effect of +/pho JPs on membrane fluidity. We measured changes in lipid diffusion coefficient (ΔD) before and after the bilayers interacted with particles using fluorescence recovery after photobleaching (FRAP). We found that, over the range of 0-20 pM, the +/pho JPs had little effect on the fluidity of the non-defect portions of DOPA lipid bilayers (**Fig. 2c**). However, by contrast, for pure DOPC bilayers, the particles did cause a significant decrease in bilayer fluidity. We have previously reported that, for pure DOPC bilayers, particles cause a global loss of lipids from the entire bilayers.[9] But this appears not the case for DOPA bilayers, based on the unaffected lipid diffusion in areas surrounding the defects. It is likely that +/pho JPs interact with DOPA bilayers in a more localized fashion, due to the strong electrostatic attraction, by drawing lipids only from the immediate region where they are adsorbed.

To better understand the interaction between +/pho JPs and DOPA bilayers, we fluorescently labeled both the lipid bilayers and the particles, and started imaging their dynamics when the particles were added. We observed two distinctly different defect-forming processes that depended on the DOPA fraction in the bilayers. Planar bilayers with 5% and 10% DOPA content exhibited many hemispheric lipid caps. The

+/pho JPs were observed to adsorb on both the lipid caps and the planar bilayer areas. Within seconds after particle landing, the lipid caps disappeared in a manner reminiscent of bubbles bursting. Defects appeared immediately at the same locations (**Fig. 3a,b** and **Movie S1**). A majority of the defects in the bilayers with 5% and 10% DOPA content were formed via this process. In contrast, fewer defects were caused by particles adsorbed on the planar bilayer areas, and those defects typically did not appear until a few minutes after the adsorption of the particle. According to a previous study, the lipid caps are enriched in DOPA.[56] The caps therefore likely served as localized "hotspots" that are more electrostatically attractive for the +/pho JPs than the surrounding planar area. Electrostatic attraction alone, however, is not sufficient to cause the lipid caps to "burst". In control experiments, a similar phenomenon was not observed for homogeneous cationic nanoparticles (**Fig. S2**). This result demonstrates that the hydrophobicity of the Janus particles is required to induce the "bursting" membrane disruption. Bilayers with 0.2% and 1% DOPA content behaved differently than 5% and 10% DOPA bilayers. No lipid caps were observed to form, and defects appeared long after particle adsorption on planar areas (**Fig. 3c,d**). Defects formed via the two different processes exhibited different morphologies: the ones formed after the "bursting" of lipid caps were relatively round and smooth on the edge, but the ones formed on the planar areas of bilayers exhibited more branching features. This explains the different defect morphologies shown in **Fig. 1**.

We next sought to determine which side of the +/pho JPs preferably interacts with the DOPA bilayers. Our previous study has shown that the hydrophobic hemisphere of +/pho JPs faces zwitterionic DOPC lipid bilayers as the hydrophobic attraction extracts lipids from the bilayer to the particles.[9] But the particle orientation could be altered on DOPA bilayers due to the strong electrostatic attraction. The principle of our measurement of particle orientation, as described previously,[9] is that fluorescently labeled +/pho JPs emit different intensities of light depending on their orientation. The gold caps on one side block the fluorescence emission from the other side. We measured the fluorescence intensity of single particles on the planar areas of 5 and 10% DOPA bilayers from fluorescence images. We found that the particles on DOPA bilayers exhibited fluorescence intensity comparable to that measured on hydrophobic substrates, but a much weaker intensity compared to that measured on hydrophilic glass substrates (**Fig. 4**). This indicates that the +/pho JPs were in contact with the bilayers with their hydrophobic side. However, particles exhibited a larger variation in fluorescence intensity on 5% and 10% DOPA bilayers than on pure DOPC bilayers. This indicates that particles on DOPA bilayers have a more random distribution of orientations, which is likely due to the stronger electrostatic attraction between the charged side of particles and the bilayers.

The results altogether indicate that the DOPA content has two somewhat opposite effects on the interaction between +/pho JPs and the bilayers. On the one hand, increasing DOPA content leads to faster particle adsorption and more formation of DOPA-rich cap structures, both of which promote the formation of bilayer defects. On the other hand, stronger electrostatic attraction at higher DOPA content hinders the re-orientation of +/pho JPs and therefore reduces the hydrophobic attraction between the particles and the bilayers, which drives the bilayer defects. This provides an explanation for the non-monotonic dependence of bilayer defects on DOPA content.

2. The effects of cationic lipids on the interaction between +/pho JPs and lipid bilayers

We next investigated the interaction between positively charged lipid bilayers and +/pho JPs. The cationic lipid DOTAP was included in DOPC bilayers at varied molar fractions. DOTAP has a cationic headgroup but shares the same unsaturated alkyl chains as DOPC. The DOTAP bilayers were first made in phosphate buffers (pH = 7), as we did for DOPA bilayers. To avoid particle aggregation, the buffer was then replaced with de-ionized water prior to the addition of +/pho JPs. We observed the bilayer morphology at 70 minutes after interaction with the particles (**Fig. 5**). We found, first, that the +/pho JPs induce defects in all DOTAP bilayers. Higher DOTAP content in bilayers lowered the threshold particle concentration needed to induce defects. A 20 pM concentration of particles was needed to cause defects in 1% DOTAP bilayers and pure

DOPC bilayers, but 10 pM was sufficient for 5% and higher DOTAP compositions. Second, compared to other compositions, 5% DOTAP exhibited the most significant defect formation. With 20 pM particles, the surface coverage of defects was 94.1 ± 0.8 % for 5% DOTAP bilayers, with minimal intact bilayer left (**Fig. 6a**). In contrast, the surface coverage of defects was only 26.9 ± 1.2%, 16.0 ± 0.8% and 26.0 ± 2.3% for 1%, 10% and 20% DOTAP bilayers, respectively, under the same experimental conditions. The fluidity properties of the bilayer paralleled to the surface coverage of defects. The entire 5% DOTAP bilayers lost membrane fluidity after interaction with the +/pho JPs, whereas other DOTAP bilayers remained largely fluidic (**Fig. 6b**). We summarized the results in a phase diagram, using both defect surface coverage and lipid diffusion changes as indicators of the integrity of the bilayer (**Fig. 6d**). The bilayer disruption induced by +/pho JPs depends non-monotonically on its content of DOTAP. The disruption to bilayers peaked at 5% DOTAP but decreased at higher DOTAP fractions. Pure cationic nanoparticles within the concentration range used here failed to induce any defects, confirming that the hydrophobic attraction is required for the disruption to the DOTAP bilayers, as with the anionic DOPA and zwitterionic DOPC bilayers.

To understand the causes of the phenomenon, we imaged both the +/pho JPs and the DOTAP bilayers during their interactions, again using florescence microscopy. A majority of the particles either did not adsorb on the bilayers or quickly detached after adsorption (**Movie S2, S3**). We found, by plotting the number of adsorbed particles per unit of surface area as a function of time, that the associate rate constant (k_a) is 5770 ± 30 M^{-1} s^{-1} on 5 % DOTAP. This is a significant decrease compared to that on pure DOPC bilayers (24700 ± 180 M^{-1} s^{-1}) (**Fig. S3**). At higher DOTAP content, k_a decreased further to 2970 ± 220 M^{-1} s^{-1} for 10 % DOTAP and 1170 ± 90 M^{-1} s^{-1} for 20 % DOTA. The decreased particle adsorption indicates stronger electrostatic repulsion between the particles and the bilayer at higher DOTAP content. The small population of +/pho JPs that did adsorb on the bilayers were oriented with their hydrophobic caps facing the bilayers, as indicated by their weak fluorescence emission (**Fig. 6c**). Interestingly, those adsorbed particles became sites for particle aggregation after the formation of defects (**Movie S3**).

The cause for the extensive defect formation peaked at 5% DOTAP is unclear. The defects were mainly driven by hydrophobic interactions, but the extent of the defect formation, we propose, is modified by two effects from the cationic DOTAP lipids. One is the electrostatic repulsion between the DOTAP bilayers and particles. Higher DOTAP content leads to fewer +/pho JPs adsorbed on the bilayers and hence less defect formation. A second and countering effect might come from the instability in the DOTAP bilayers. The fractal shape of the defects formed in 5% DOTAP bilayers (**Fig. 5**) is characteristic of an unstable two-dimensional domain growth process in lipid bilayers.[57] Previous studies, both experimental and computational, have shown that DMTAP, a cationic lipid with the same headgroup as DOTAP, can change the stability of zwitterionic DMPC lipids in bilayers by affecting the orientation of PC headgroups and molecular packing of zwitterionic lipids surrounding the cationic lipids.[58-60] Similar localized structural changes are likely in the DOTAP/DOPC bilayers used here, which may intensify the defects induced by +/pho JPs and leads to the prominent defect formation in 5% DOTAP bilayers.

Conclusions

We have shown previously that amphiphilic cationic/hydrophobic Janus nanoparticles at the pM concentration level disrupt zwitterionic lipid bilayers by inducing holes in them. In this study, we investigated the role of charged lipids in the interaction between such nanoparticles and bilayers. For both cationic and anionic bilayers, we found that +/pho JPs in the 10-20 pM concentration range can induce defects in both types of bilayers. As with zwitterionic lipid bilayers, hydrophobic attraction between the +/pho JPs and the charged bilayers, regardless of the sign of the charges, causes lipid loss and subsequently defects in bilayers. The exact nature of the defect formation, however, is dependent on the charged lipid composition in a non-monotonic manner. We can draw the following key conclusions: (1) +/pho JPs cause defects in charged lipid bilayers at lower threshold concentrations than in zwitterionic bilayers, regardless of whether the electrostatic force is attractive or repulsive. (2) The electrostatic attraction between particles

and anionic DOPA bilayers enhances particle adsorption kinetics and lowers the threshold particle concentration needed to induce defects, but also leads to more localized membrane disruption. This was most obvious in the case of 5 and 10% DOPA bilayers. In these bilayers, +/pho JPs induced defects by preferably adsorbing onto DOPA-rich lipid cap structures formed on the bilayers and inducing the "bursting" of such lipid structures. (3) For cationic DOTAP bilayers, we found that bilayer defects were most extensive at 5% content of DOTAP, but less at either lower or higher DOTAP compositions. The fractal shape of the defects formed in DOTAP bilayers implies an unstable two-dimensional domain growth process induced by the +/pho JPs.

This study revealed the complex roles played by charged lipids in particle-membrane interactions. We do not yet fully understand many phenomena in the system. The complexity comes from that fact that charged lipids influence not only the direct electrostatic interaction of bilayers with particles, but also the structural properties of the bilayer. This structural influence modifies the overall particle-bilayer interaction. Although the fundamental driving forces are electrostatic and hydrophobic interactions, due to these sources of complexity, the defects induced by +/pho JPs vary significantly depending on lipid bilayer composition. It is vital to consider this complexity when establishing models to predict the interaction between particles and biomembranes of various compositions. Charged lipids are a key component in the cell membranes of living organisms. Thus, our findings may help understand how the charged lipids influence the biological impact of nanoparticles, particularly those with heterogeneous surface chemistries.

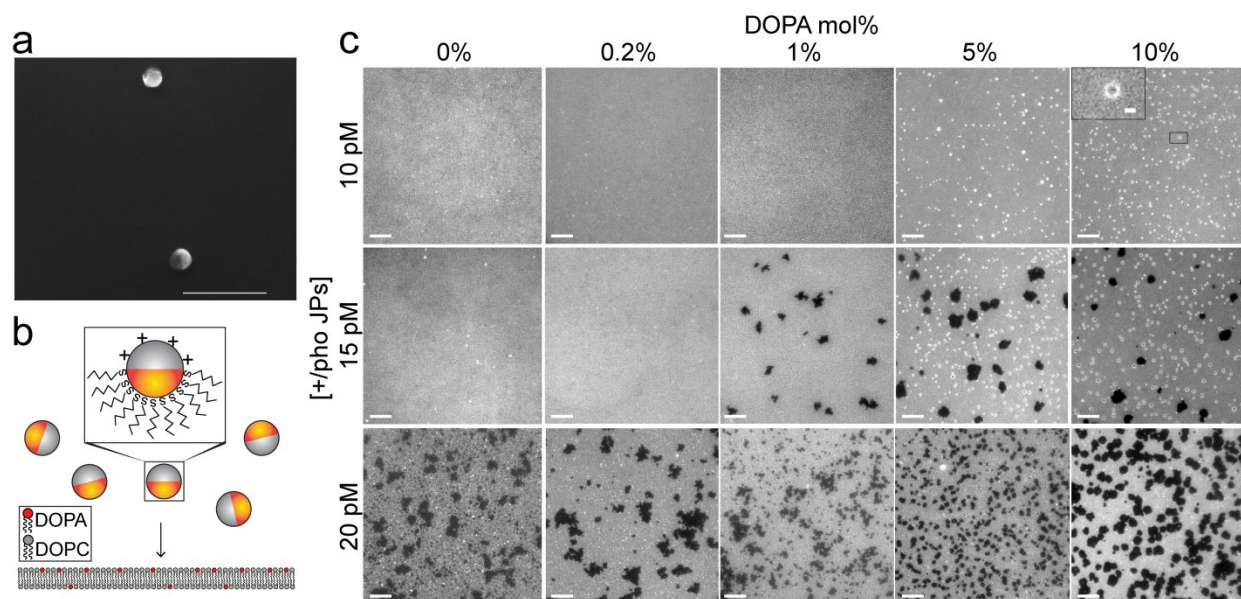## ACKNOWLEDGMENTS

Figures and Captions

Figure 1. (a) SEM image of the cationic/hydrophobic amphiphilic Janus nanoparticles. Scale bar: 500 nm. (b) Schematic illustration of the experimental system. (c) Fluorescence images showing the morphology of bilayers as a function of particle concentration and composition of DOPA lipids (mol%). The lipid caps appear as white circles and dots, and holes appear as dark areas. Inset is a zoomed in image of a lipid cap structure. All images were acquired 70 min after the addition of particles to lipid bilayers. Each image shown is representative of results from three independent samples. Scale bars: 10 μm.
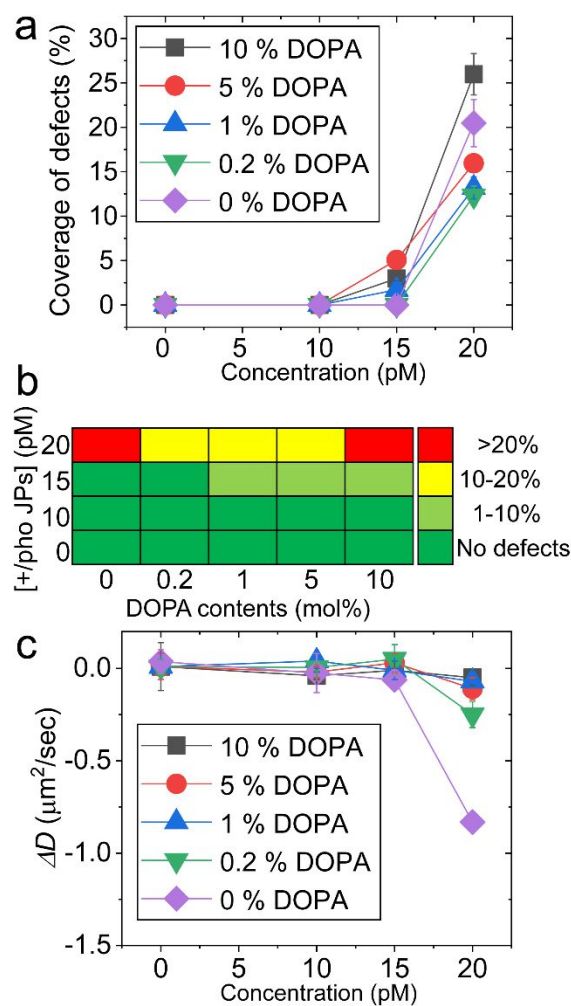
Figure 2. (a) Surface coverage of defects in bilayers plotted as a function particle concentration for different DOPA compositions. (b) A phase diagram showing the dependence of lipid bilayer morphology on DOPA composition and Janus particle concentration. The diagram is color-coded based on the average surface coverage of defects at 70 min after particle-bilayer interaction. (c) Change of lipid diffusion coefficient plotted as a function particle concentration for different DOPA compositions. Each data point in the plots shown was obtained from an average of 29 images from three independent samples.
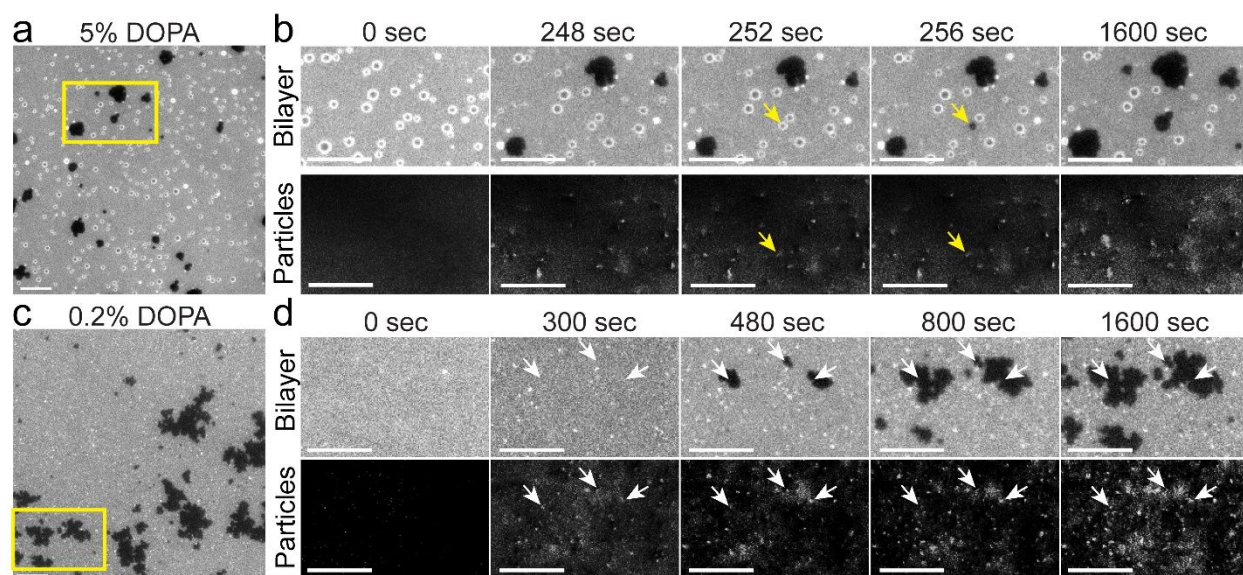
Figure 3. Dual-color fluorescence images showing Janus particles and DOPA lipid bilayers during membrane defect formation. Approximately 25% of the particles were fluorescently labeled. Particle concentration was 15 pM in (a) and (b), and 20 pM in (c) and (d). (a) and (c) are images acquired 70 min after the addition of particles. (b) and (d) are zoomed-in snapshots of a representative region as marked in (a) and (c), respectively. Yellow and white arrows highlight defect formation on lipid caps and in planar bilayer areas, respectively, after particle landing. Time-lapse images shown are representative of three independent samples. Scale bars: 10 μm.
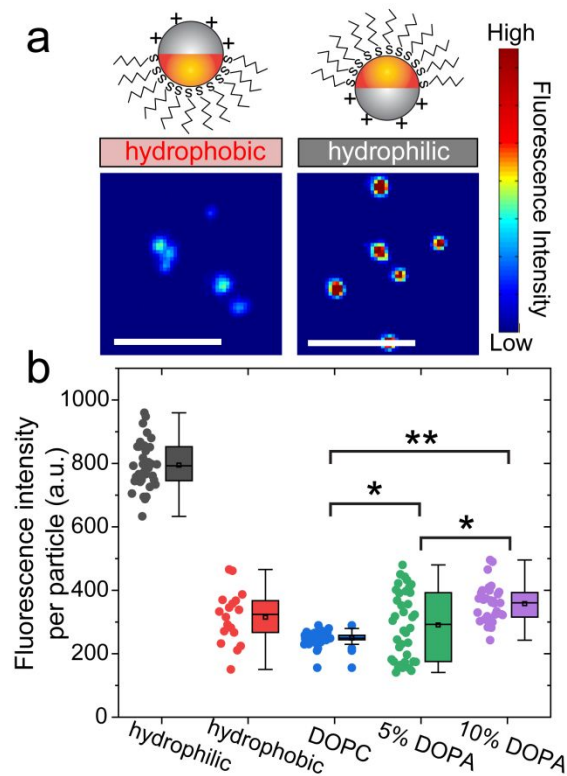
Figure 4. Quantification of Janus particle orientation on different surfaces. (a) Schematic illustration and color-coded fluorescence images showing the orientation and corresponding fluorescent intensity of Janus particles on hydrophobic and hydrophilic substrates. Scale bars: 5 μm (b) Scattered plot showing average fluorescence intensity per particle on different surfaces. Each data point represents measurement from a single particle. Each box plot indicates the mean (squared dot), median (horizontal line), and the interquartile range from 25 % to 75 % of the corresponding data set. Each set of data shown was obtained from two independent samples. Statistical significance is highlighted by *p*-values (student's t test) as follows: *p<0.01, **p<0.001.
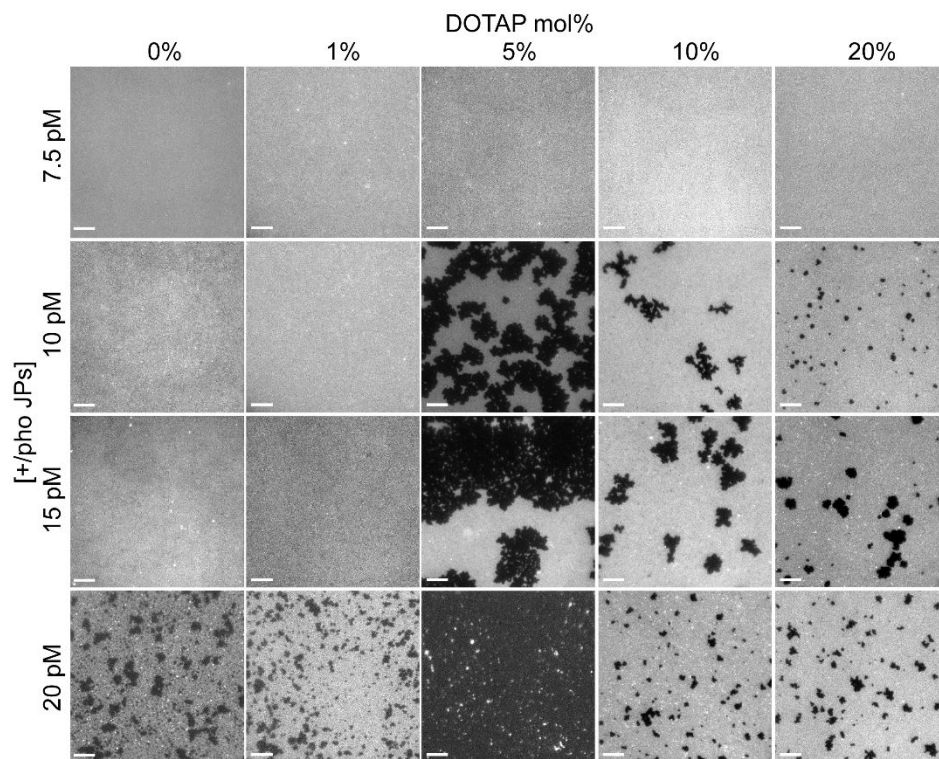
Figure 5. Fluorescence images showing the morphology of bilayers as a function of particle concentration and composition of DOTAP lipids (mol%). All images were acquired 70 min after the addition of particles. Each image shown is representative of results from three independent samples. Scale bars: 10 μm.
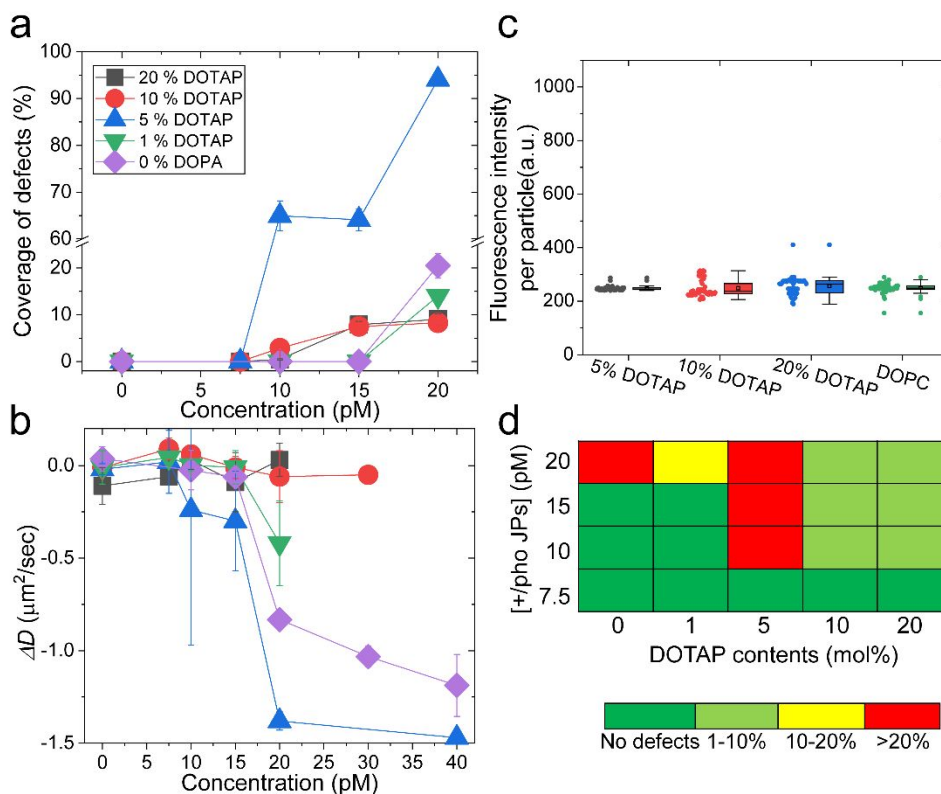
Figure 6. (a) Surface coverage of defects in bilayers and (b) change of lipid diffusion coefficient, both as a function particle concentration for different DOTAP compositions. (c) Quantification of particle orientation on various lipid bilayers as indicated. (d) A "phase" diagram showing the dependence of lipid bilayer morphology on DOTAP composition and Janus particle concentration. The diagram is color-coded based on the average surface coverage of defects at 70 min after particle-bilayer interaction. Each data point shown in (a) and (b) was obtained from an average of 29 images from three independent samples. Each set of data shown in (c) was obtained from two independent samples.

REFERENCES

1. A. Nel, T. Xia, L. Madler and N. Li, *Science*, 2006, **311**, 622-627.
2. R. Landsiedel, L. Ma-Hock, A. Kroll, D. Hahn, J. Schnekenburger, K. Wiench and W. Wohlleben, *Adv Mater*, 2010, **22**, 2601-2627.
3. B. Pelaz, G. Charron, C. Pfeiffer, Y. L. Zhao, J. M. de la Fuente, X. J. Liang, W. J. Parak and P. del Pino, *Small*, 2013, **9**, 1573-1584.
4. A. M. Nystrom and B. Fadeel, *J Control Release*, 2012, **161**, 403-408.
5. Q. X. Mu, G. B. Jiang, L. X. Chen, H. Y. Zhou, D. Fourches, A. Tropsha and B. Yan, *Chem Rev*, 2014, **114**, 7740-7781.
6. J. M. Anderson, *Annu Rev Mater Res*, 2001, **31**, 81-110.
7. B. D. Ratner and S. J. Bryant, *Annu Rev Biomed Eng*, 2004, **6**, 41-75.
8. B. Jing and Y. Zhu, *J Am Chem Soc*, 2011, **133**, 10983-10989.
9. K. Lee, L. Zhang, Y. Yi, X. Wang and Y. Yu, *ACS Nano*, 2018, **12**, 3646-3657.
10. K. Lee and Y. Yu, *Langmuir*, 2018, **34**, 12387-12393.
11. B. Jing, R. C. Abot and Y. Zhu, *J Phys Chem B*, 2014, **118**, 13175-13182.
12. X. Xiao, G. A. Montano, T. L. Edwards, A. Allen, K. E. Achyuthan, R. Polsky, D. R. Wheeler and S. M. Brozik, *Langmuir*, 2012, **28**, 17396-17403.
13. B. X. Jing and Y. X. Zhu, *J Am Chem Soc*, 2011, **133**, 10983-10989.
14. R. C. Van Lehn, M. Ricci, P. H. J. Silva, P. Andreozzi, J. Reguera, K. Voitchovsky, F. Stellacci and A. Alexander-Katz, *Nat Commun*, 2014, **5**.
15. J. H. Gao, O. Zhang, J. Ren, C. L. Wu and Y. B. Zhao, *Langmuir*, 2016, **32**, 1601-1610.
16. B. X. Jing, R. C. T. Abot and Y. X. Zhu, *J Phys Chem B*, 2014, **118**, 13175-13182.
17. P. R. Leroueil, S. A. Berry, K. Duthie, G. Han, V. M. Rotello, D. Q. McNerny, J. R. Baker, Jr., B. G. Orr and M. M. Holl, *Nano Lett*, 2008, **8**, 420-424.
18. B. Wang, L. F. Zhang, S. C. Bae and S. Granick, *P Natl Acad Sci USA*, 2008, **105**, 18171-18175.
19. R. P. Carney, Y. Astier, T. M. Carney, K. Voitchovsky, P. H. J. Silva and F. Stellacci, *Acs Nano*, 2013, **7**, 932-942.
20. Y. Roiter, M. Ornatska, A. R. Rammohan, J. Balakrishnan, D. R. Heine and S. Minko, *Nano Lett*, 2008, **8**, 941-944.
21. A. Mecke, D. K. Lee, A. Ramamoorthy, B. G. Orr and M. M. B. Holl, *Langmuir*, 2005, **21**, 8588-8590.
22. A. Mecke, I. J. Majoros, A. K. Patri, J. R. Baker, M. M. B. Holl and B. G. Orr, *Langmuir*, 2005, **21**, 10348-10354.
23. O. Boussif, F. Lezoualch, M. A. Zanta, M. D. Mergny, D. Scherman, B. Demeneix and J. P. Behr, *P Natl Acad Sci USA*, 1995, **92**, 7297-7301.
24. E. Wagner, *Accounts Chem Res*, 2012, **45**, 1005-1013.
25. Y. Ishitsuka, L. Arnt, J. Majewski, S. Frey, M. Ratajczek, K. Kjaer, G. N. Tew and K. Y. C. Lee, *J Am Chem Soc*, 2006, **128**, 13123-13129.
26. E. F. Palermo, D. K. Lee, A. Ramamoorthy and K. Kuroda, *Journal of Physical Chemistry B*, 2011, **115**, 366-375.
27. A. Mecke, D. K. Lee, A. Ramamoorthy, B. G. Orr and M. M. B. Holl, *Biophys J*, 2005, **89**, 4043-4050.
28. N. Papo and Y. Shai, *Peptides*, 2003, **24**, 1693-1703.
29. A. El-Sayed, S. Futaki and H. Harashima, *Aaps J*, 2009, **11**, 13-22.
30. K. A. Henzler-Wildman, G. V. Martinez, M. F. Brown and A. Ramamoorthy, *Biochemistry-Us*, 2004, **43**, 8459-8469.
31. A. Demuro, E. Mina, R. Kayed, S. C. Milton, I. Parker and C. G. Glabe, *J Biol Chem*, 2005, **280**, 17294-17300.
32. K. V. R. Reddy, R. D. Yedery and C. Aranha, *Int J Antimicrob Ag*, 2004, **24**, 536-547.

33. M. P. Pfeil, A. L. B. Pyne, V. Losasso, J. Ravi, B. Lamarre, N. Faruqui, H. Alkassem, K. Hammond, P. J. Judge, M. Winn, G. J. Martyna, J. Crain, A. Watts, B. W. Hoogenboom and M. G. Ryadnov, *Sci Rep-Uk*, 2018, **8**.
34. H. Pera, T. M. Nolte, F. A. M. Leermakers and J. M. Kleijn, *Langmuir*, 2014, **30**, 14581-14590.
35. B. Wang, L. Zhang, S. C. Bae and S. Granick, *Proc Natl Acad Sci U S A*, 2008, **105**, 18171-18175.
36. P. R. Leroueil, S. A. Berry, K. Duthie, G. Han, V. M. Rotello, D. Q. McNerny, J. R. Baker, B. G. Orr and M. M. B. Holl, *Nano Lett*, 2008, **8**, 420-424.
37. S. P. Hong, A. U. Bielinska, A. Mecke, B. Keszler, J. L. Beals, X. Y. Shi, L. Balogh, B. G. Orr, J. R. Baker and M. M. B. Holl, *Bioconjugate Chem*, 2004, **15**, 774-782.
38. S. Tatur, M. Maccarini, R. Barker, A. Nelson and G. Fragneto, *Langmuir*, 2013, **29**, 6606-6614.
39. L. Lai, S. J. Li, J. Feng, P. Mei, Z. H. Ren, Y. L. Chang and Y. Liu, *Langmuir*, 2017, **33**, 2378-2386.
40. E. C. Cho, J. Xie, P. A. Wurm and Y. Xia, *Nano Lett*, 2009, **9**, 1080-1084.
41. V. V. Ginzburg and S. Balijepailli, *Nano Lett*, 2007, **7**, 3716-3722.
42. R. Gupta and B. Rai, *Sci Rep-Uk*, 2017, **7**.
43. H. M. Ding, W. D. Tian and Y. Q. Ma, *Acs Nano*, 2012, **6**, 1230-1238.
44. J. Q. Lin, H. W. Zhang, Z. Chen and Y. G. Zheng, *Acs Nano*, 2010, **4**, 5421-5429.
45. L. T. Yan and X. B. Yu, *Macromolecules*, 2009, **42**, 6277-6283.
46. R. Chelladurai, K. Debnath, N. R. Jana and J. K. Basu, *Langmuir*, 2018, **34**, 1691-1699.
47. Y. Li, X. R. Zhang and D. P. Cao, *Soft Matter*, 2014, **10**, 6844-6856.
48. R. C. Van Lehn and A. Alexander-Katz, *Soft Matter*, 2014, **10**, 648-658.
49. Y. F. Li, X. J. Li, Z. H. Li and H. J. Gao, *Nanoscale*, 2012, **4**, 3768-3775.
50. R. C. Van Lehn and A. Alexander-Katz, *Soft Matter*, 2011, **7**, 11392-11404.
51. S. Pogodin, N. K. H. Slater and V. A. Baulin, *Acs Nano*, 2012, **6**, 1308-1313.
52. H. M. Ding and Y. Q. Ma, *Nanoscale*, 2012, **4**, 1116-1122.
53. A. Alexeev, W. E. Uspal and A. C. Balazs, *Acs Nano*, 2008, **2**, 1117-1122.
54. I. Salib, X. Yong, E. J. Crabb, N. M. Moellers, G. T. McFarlin, O. Kuksenok and A. C. Balazs, *Acs Nano*, 2013, **7**, 1224-1238.
55. K. Lee, L. Y. Zhang, Y. Yi, X. Q. Wang and Y. Yu, *Acs Nano*, 2018, **12**, 3646-3657.
56. L. R. Cambrea and J. S. Hovis, *Biophys J*, 2007, **92**, 3587-3594.
57. A. E. McKiernan, T. V. Ratto and M. L. Longo, *Biophys. J.*, 2000, **79**, 2605-2615.
58. V. Levadny and M. Yamazaki, *Langmuir*, 2005, **21**, 5677-5680.
59. A. A. Gurtovenko, M. Patra, M. Karttunen and I. Vattulainen, *Biophys. J.*, 2004, **86**, 3461-3472.
60. L. Zhang, T. A. Spurlin, A. A. Gewirth and S. Granick, *The Journal of Physical Chemistry B*, 2006, **110**, 33-35.

Table of Contents (TOC)